(Invited Paper)

Superlattice barrier infrared detector development at the Jet Propulsion Laboratory

David Z. Ting*, Alexander Soibel, Sir B. Rafol, Jean Nguyen, Linda Höglund, Arezou Khoshakhlagh, Sam A. Keo, John K. Liu, Jason M. Mumolo, Sarath D. Gunapala

Jet Propulsion Laboratory, California Institute of Technology, 4800 Oak Grove Drive, Pasadena, California, USA 91109-8099

ABSTRACT

We report recent efforts in achieving state-of-the-art performance in type-II superlattice based infrared photodetectors using the barrier infrared detector architecture. We used photoluminescence measurements for evaluating detector material and studied the influence of the material quality on the intensity of the photoluminescence. We performed direct noise measurements of the superlattice detectors and demonstrated that while intrinsic 1/*f* noise is absent in superlattice heterodiode, side-wall leakage current can become a source of strong frequency-dependent noise. We developed an effective dry etching process for these complex antimonide-based superlattices that enabled us to fabricate single pixel devices as well as large format focal plane arrays. We describe the demonstration of a 1024×1024 pixel long-wavelength infrared focal plane array based the complementary barrier infrared detector (CBIRD) design. An 11.5 μm cutoff focal plane without anti-reflection coating has yielded noise equivalent differential temperature of 53 mK at operating temperature of 80 K, with 300 K background and cold-stop. Imaging results from a recent 10 μm cutoff focal plane array are also presented.

Keywords: unipolar barrier, heterostructure, infrared, photodetector, superlattice

1. INTRODUCTION

The closely lattice-matched InAs/GaSb/AlSb (antimonide) material system offers tremendous flexibility in realizing high-performance infrared detectors. Antimonide-based alloy and type-II superlattice [1] infrared absorbers can be customized to have cutoff wavelengths ranging from the short wave infrared (SWIR) to the very long wave infrared (VLWIR). The type-II InAs/Ga(In)Sb superlattices have several key properties that make them favorable for infrared detection. Their band gaps can be made arbitrarily small [2]. They have sufficient absorption strength to attain high quantum efficiency [3]. They are less susceptible to band-to-band tunneling when compared to bulk material [3,4]. They are also capable of achieving reduced Auger recombination [5,6]. The antimonides can also be used in constructing sophisticated heterostructures to enable advanced infrared photodetector designs. In particular, they facilitate the construction of unipolar barriers, which can block one carrier type but allow the un-impeded flow of the other. Unipolar barriers are used to implement the barrier infra-red detector (BIRD) design for increasing the collection efficiency of photo-generated carriers, and reducing dark current generation without impeding photocurrent flow. Heterostructure superlattice detectors that make effective use of unipolar barriers have demonstrated strong reduction of generation-recombination (G-R) dark current due to Shockley-Read-Hall (SRH) processes. Despite relatively short lifetimes found

* David.Z.Ting@jpl.nasa.gov; Ph: +1.818.354.1549; FAX: +1.818.393.4663

in present day superlattice material, the higher absorber doping levels afforded by immunity to tunneling has led to reduced diffusion dark current. The dark current characteristics of type-II superlattice based single element LWIR detectors are now approaching that of the state-of-the-art MCT detector. However, noise measurements highlight the need for surface leakage suppression, which can be tackled by improved etching, passivation, and device design. The various aspects of type-II superlattice infrared detectors have been covered in detail in review articles by Fuchs *et al*. [7], Bürkle and Fuchs [8], Razeghi and Mohseni [9], and Ting *et al*. [10], as well as in the book by Rogalski [11]. In this paper, we discuss some recent development in the area of type-II superlattice based infrared detectors at the Jet Propulsion Laboratory (JPL).

2. THE COMPLEMENTARY BARRIER INFRARED DETECTOR

2.1 Theoretical considerations

Many of the key properties the type-II superlattice are readily revealed by examining the band structure. Figure 1 shows the band structure of a (22,6)-InAs/GaSb LWIR superlattice, calculated using an enhanced effective bond orbital model [12] (Cartoixà et al., 2003) that accounts for bulk-inversion asymmetry (BIA). The spin splittings in the valence subbands along [100] are due to BIA effects. A prominent feature of the superlattice band structure that distinguishes it from that of the typical bulk semiconductor is the splitting of the highest heavy hole band (hh1) and the highest light hole band (lh1) at the zone center. While the infrared absorption edge is determined by the gap between the lowest conduction band (c1) and the hh1 band, the electron effective mass is determined by the c1-lh1 gap. In unstrained bulk semiconductors, the two gaps are the same. In the superlattice, the larger c1-lh1 gap leads to a substantially larger electron effective mass relative to that of a bulk semiconductor with the same fundamental band gap. The larger electron effective mass is beneficial for reducing band-to-band tunneling as well as trap assisted tunneling. It is also favorable for reducing diffusion dark current.

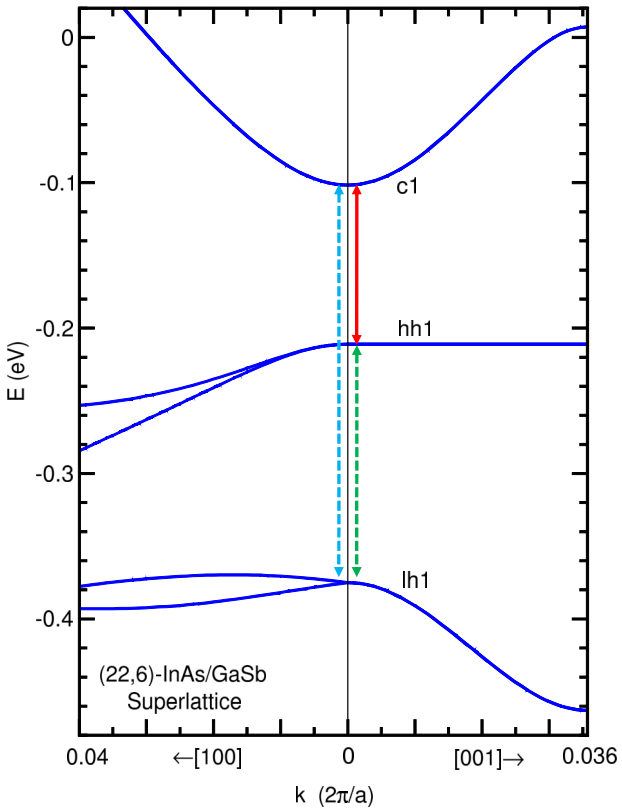

Figure 1. Conduction and valence subband structure emanating from the zone center along an in-plane direction (k_x or [100]) and the growth direction (k_z or [001]), for an InAs/GaSb long wavelength infrared superlattice. Each superlattice period consists of L_z=28 monolayers (MLs), with 22 MLs of InAs and 6 MLs of GaSb.

The splitting of the hh1 and lh1 subbands can also result in the suppression of the Auger-7 recombination process, in which a minority electron recombines with a majority hole across the band gap, while exciting another majority hole deeper into the valence bands. In the case of the LWIR InAs/GaSb superlattice shown in Figure 1, because the hh1-lh1 separation is actually larger than the c1-hh1 separation (superlattice band gap), energy and momentum conservation considerations render it difficult to find matching hh1-lh1 transitions for c1-hh1 transitions, thereby suppressing Auger-7 events. Note that the degree to which a given type-II superlattice can benefit from Auger suppression depends on the details of the band structure and doping levels; the subject has been studied extensively by Grein and co-workers [5,13,14, 15,16].

Another prominent feature of the band structure shown in Figure 1 is that the hh1 band is nearly dispersionless along [001], or the growth direction. Both the dispersionless hh1 band structure and the increased electron effective mass contribute to a larger joint density of states (JDOS). This results in a larger absorption coefficient, which, to first order, is directly proportional to the JDOS. This helps to compensate for the small optimal matrix element disadvantage inherent in type II superlattices.

The band structure in Figure 1 reveals important information about carrier transport properties which can affect detector design. We note that the c1 subband shows strong dispersion along both the growth (z) and an in-plane direction (x), while the hh1 band is highly anisotropic and appears nearly dispersionless along the growth (transport) direction. It is interesting to note that the electron effective mass along the growth direction is quite small (even slightly smaller than in-plane electron effective mass), and the superlattice conduction band structure near the zone center is approximately isotropic. This is in stark contrast to the highly anisotropic valence band structure. Recalling that carrier group velocity is given by $\mathbf{v} = \nabla_{\mathbf{k}} E(\mathbf{k}) / \hbar$, where $E(\mathbf{k})$ describes the band structure, we would expect very low hole mobility and diffusivity along the growth direction. Therefore, for this LWIR superlattice absorber, detector designs based on hole transport would be rather unfavorable.

To understand the physical origin for the near-isotropy in the conduction band, and the extreme anisotropy of the valence band, in Figure 2 we shows the schematic energy band diagrams the (22,6)-InAs/GaSb superlattice, along with the positions of the c1, hh1, and lh1 states relative to the InAs and GaSb band gaps. We note that the c1 level of the (22,6)-InAs/GaSb superlattice is in the broken gap region (i.e., in the energy range that does not overlap with either of the InAs and GaSb band gaps). Therefore an electron in the c1 level can travel along the growth direction without having to tunnel through any forbidden band gap regions. This explains the low electron effective mass in the growth direction. On the other hand, we note in Figure 2 that the hh1 level is also in the broken gap region. Then why is the hh1 effective mass so large along the growth direction? The reason has to do with the symmetry of the heavy-hole states. In the c1 level, the quantized level in the InAs conduction band quantum well can couple to the propagating light-hole states in the GaSb layers. For the hh1 level, by symmetry the quantized heavy-hole states in the GaSb quantum well cannot couple to the propagating conduction band states in InAs despite having the same energy, and instead has to couple to evanescent states with large wave vectors in InAs. As a result, the quantized heavy hole states in neighboring GaSb quantum wells are essentially isolated from one another, leading to the nearly dispersionless hh1 band.

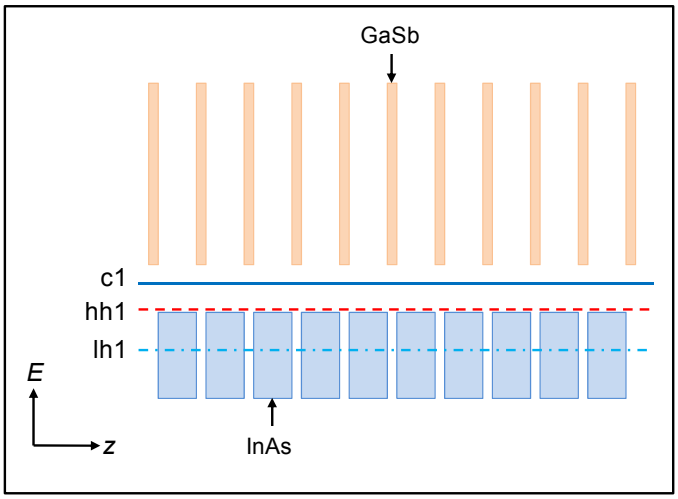

Figure 2. Schematic energy band diagrams of the (22,6)-InAs/GaSb superlattice along with the c1, hh1, and lh1 energy levels. The energy band gaps of InAs and GaSb are indicated by shaded solid rectangles.

2.2 CBIRD design and characterization

Superlattice infrared detectors based on heterojunction designs, particular those based on unipolar barrier designs, have demonstrated clear advantages over their homojunction counterparts. The term "unipolar barrier" describes a barrier that can block one carrier type (electron or hole) but allows the un-impeded flow of the other [17,18,19]; the concept of the unipolar barrier has been in existence since 1963 [20,21], in connection with the double-heterostructure laser. Broadly speaking, the typical heterojunction superlattice infrared detectors are either based on the nBn/pBp/XBn design [22,23,24,25,26,27,28], or variations of the double heterojunction (DH) design. The first category includes the single-band superlattice nBn detector [29], the dual-band superlattice nBn detector [30], the superlattice pMp detector [31], and

the superlattice pBn detector [32]. The second category includes the superlattice DH structure [33,34], the p-π-M-n detector [35], and the PbIbN structure [36]. At JPL, we have been working with the complementary barrier infrared detector (CBIRD) [19] structure, which is also a variation of the DH design.

The CBIRD design, consists of an InAs/GaSb absorber SL sandwiched between an InAs/AlSb unipolar hole barrier (hB) SL, and an InAs/GaSb unipolar electron barrier (eB) SL. Figure 3 shows calculated energy band diagrams of the CBIRD device. We expect the InAs/GaSb LWIR SL to have more favorable electron transport properties. Therefore the absorber superlattice is doped lightly p-type so that we have better minority carrier (electron) mobility. A full description of the device structure is published elsewhere [19]. The device structure was grown on GaSb (100) substrate by molecular beam epitaxy (MBE). Standard contact mode optical lithography was used to fabricated large-area (220×220 μm^2 in size) devices for dark current and responsivity measurements. Detailed device results have been reported earlier [19]. Here we summarize the key points.

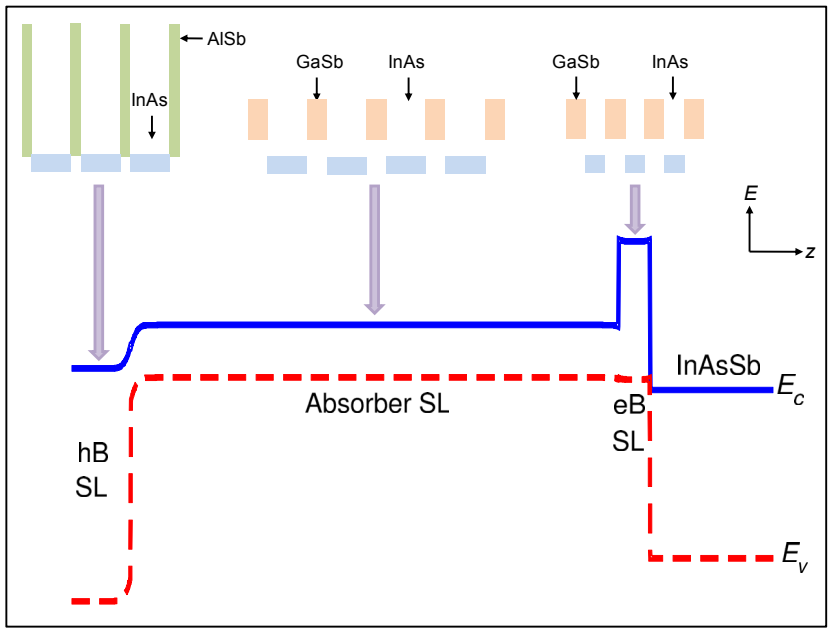

Figure 3. Calculated zero-bias energy band diagram of a complementary barrier infrared detector (CBIRD) structure, where a long-wave infrared InAs/GaSb superlattice absorber is surrounded by an InAs/AlSb superlattice hole-blocking (hB) unipolar barrier and a shorter period InAs/GaSb superlattice superlattice electron-blocking (eB) unipolar barrier. The schematic energy band diagrams of the InAs/AlSb and InAs/GaSb superlattices are shown on the top, with the direct energy band gaps of InAs, GaSb, and AlSb indicated by shaded solid rectangles.

In the device reported in Reference 19, we observed that the photoresponse increases with bias from 0 to ~0.2 V, and then plateaus for bias greater than 0.2 V. The 77 K dark current density at 0.2 V is still quite low, with a value of ~1×10^{-5} A/cm^2. Arrhenius plot shows that at 0.2 V, the dark current is diffusion limited for device temperature above ~77K. Spectral response measured under 0.2 V applied bias at 77 K shows that the device has a 10 μm cutoff (defined by 50% peak responsivity), with a peak responsivity of 1.5 A/W. We calculated the shot-noise limited black-body D^*, where the noise spectrum is determined by the measure dark current and photocurrent integrated over the 8 μm to 10 μm spectral range (the overlap between the atmospheric window and the detector cutoff). Under 0.2 V, the detector reaches 300 K BLIP operation at 86 K with a black-body BLIP D^* value of 1.1×10^{11} cm-Hz$^{1/2}$/W for f/2 optics. For 300K background with 2π field of view, the device shows a BLIP temperature of 101 K with a black-body BLIP D^* value of 2.6×10^{10} cm-Hz$^{1/2}$/W. The device has a zero-bias dynamic resistance-area product of R_0A =14,000 ohm-cm^2 at 77 K. However, since the detector is expected to operate at a higher bias (~0.2 V), a more relevant quantities is the effective resistance-area product, given by $RA_{\text{eff}} = kT/qJ_d$. Under a 0.2 V bias, the RA_{eff} for this device is 670 ohm-cm^2 at 77 K.

As a general comment, we note that superlattice heterostructure infrared detectors now have dark current performance approaching that of MCT detectors. However, MWIR and LWIR superlattices [37,38,39] studied thus far appear to have relatively short lifetimes compared to MCT [40,41]. Direct time-resolved photoluminescence measurements of an MWIR SL yielded a lifetime of 80 ns at 77K [37], while indirect inference through dark current analysis of an LWSL SL yielded a lifetime of 35 ns [39]. The question then arises as to why the observed dark current densities are not correspondingly worse for the superlattices. This turns out to be related to suppressed tunneling in superlattices. Recall

that the diffusion dark current density from the p-side of a pn diode is given by $J_{diff} = qn_i^2 L_N / (N_A \tau_n)$, where n_i is the intrinsic carrier density, L_N is the diffusion length or absorber width, whichever is shorter, N_A is the acceptor dopant density, and τ_n is the minority carrier (electron) lifetime. In a typical LWIR superlattice, the doping density is on the order of p=1 to 2×10^{16} cm^{-3}, which is considerably higher than the doping level found in the LWIR MCT (typically low 10^{15} cm^{-3}). This is possible because of tunneling current suppression in superlattices. The higher doping compensates for the shorter lifetime, resulting in relatively low diffusion dark current. To achieve the true promise of superlattices with performance exceeding that of MCT requires the understanding of the origin of the relatively short carrier lifetimes found in the current generation of superlattices, and developing methods for increasing carrier lifetime.

Optical characterization tools are invaluable in the study of the material properties of CBIRD detectors. We have been investigating CBIRD devices using two different optical characterization techniques: photoluminescence (PL) and transmission spectroscopy. We find that the absorption quantum efficiency (QE), deduced from the transmission measurements, served as a good estimate of the upper limit of the external QE, and the PL peak position was shown to correlate well with the detector cut-off wavelength. In a comparison between the PL intensity and the dark current characteristics, a good correlation between a high PL intensity and low dark current was observed, showing that the PL intensity well reflects the material quality. Also, SRH processes were identified as the limiting factor of the minority carrier lifetime of the CBIRD material studied. More details of these optical characterization results can be found in Reference 42.

We have also experimentally investigated the noise and gain of high-performance LWIR superlattice photodetectors. We compare the recently demonstrated SL heterodiode, which exhibits an electrical gain much larger than unity, with a SL photodetector without gain to show that the electrical gain in these devices originates from the device structure rather than from the superlattice absorber. We directly measure the noise spectra of high performance superlattice photodiodes, and demonstrated that intrinsically SL photodetectors do not exhibit 1/*f* noise. At the same time, our measurements clearly show that sidewall leakage current not only increases the shot noise by contributing to higher dark current but more importantly, it also introduces additional frequency dependent noise (potentially *1/f* noise), resulting in much higher noise in the detector. The 1/*f* noise has been extensively studied in p-n junctions. In particular, in MCT photodiodes, 1/*f* noise has been often associated with modulation of the surface generation currents induced by fluctuations of the surface potential. While the mechanisms of the surface leakage current in the Sb-based SL photodiodes are not completely understood yet, evidently the surfaces current can be a source of extraneous noise in these devices similar to MCT detectors. Since strong frequency-dependent noise can be generated by sidewall leakage current, it is important to fabricate the high performance SL detectors and focal plane array (FPA) using the technology that can minimize the mesa side-wall leakage current. One way to achieve this result is by development of reliable sidewall passivation that can suppress the leakage current and prevent the onset of frequency-dependent noise. More details of these noise and gain studies can be found in Reference 43.

We have also developed a dry-etch technique for pixel isolation for achieving low surface leakage for LWIR superlattice detectors. The surface leakage was reduced through the etching mechanism by minimizing the amount of differential etching and removing unwanted native oxides, byproducts, and contaminants on the sidewalls. The advantages to both chlorine-based and methane-based plasmas were exploited and combined to achieve over two orders of magnitude improvement in dark current compared to diodes etched with BCl_3/Ar. The $CH_4/H_2/BCl_3/Cl_2$/Ar etch exhibited comparable electrical performance to wet etched samples, with great improvements in structural properties. Near-vertical, smooth sidewalls with minimal dielectric mask erosion were achieved with good anisotropy resulting in more than three times higher fill factor. These performance enhancements allow small pixel size, large format LWIR FPAs to become more realizable. More details of the dry-etch technique can be found in Reference 44.

3. CBIRD FOCAL PLANE ARRAY DEVELOPMENT

This high-performance CBIRD device reported in Reference 19 has an N-p junction near the top surface. It collects electrons at the detector top contact and requires an n-on-p (or top positive polarity) read out integrated circuit (ROIC). The most commonly available ROICs are for p-on-n devices, which would need to operate with a reversed CBIRD

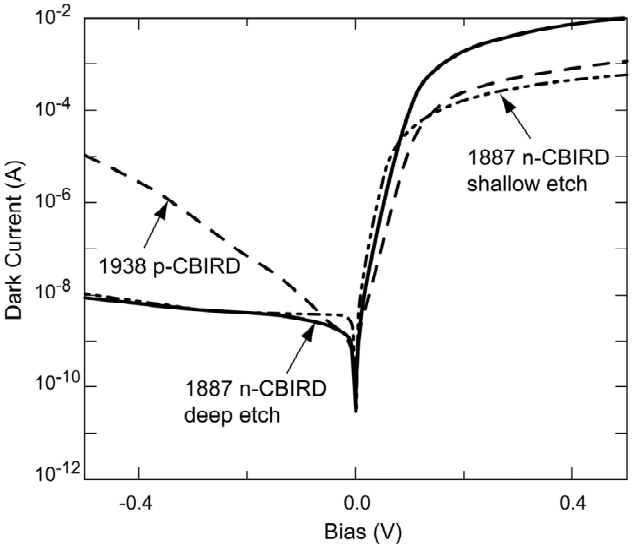

Figure 4. Dark current as a function of bias of 200 μm diameter n-CBIRD and p-CBIRD devices at 77K operating temperature. The n-CBIRDs are reverse biased under positive bias; we reflected their I-V curves about the vertical axis for easy comparison with the p-CBIRD.

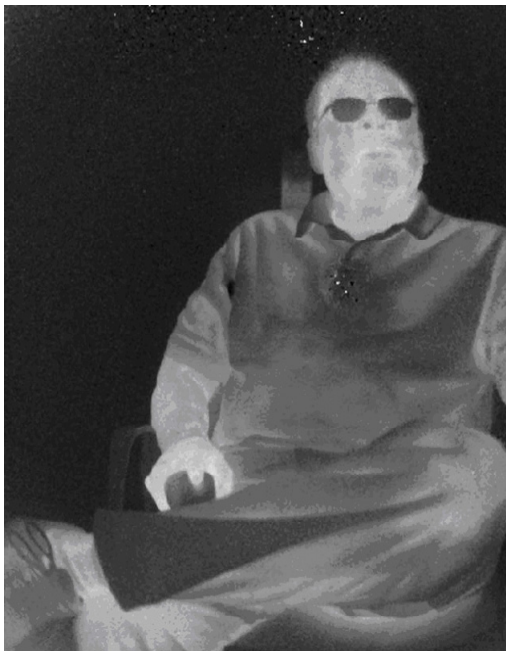

Figure 5 An image taken with the LWIR p-CBIRD FPA.

device structure that collects holes from the top. We call the top electron and hole collecting devices n-CBIRD and p-CBIRD, respectively. We have grown both n-CBIRDs and p-CBIRDs on GaSb wafers. The epitaxially grown material was processed into 200 μm diameter mesa photodiode test structures using dry etch processing. The dark current-voltage characteristics of these test devices are shown in Figure 4. Structurally the p-CBIRD is the n-CBIRD grown in reverse order, and thus should have very similar I-V characteristics. However, while the reverse-bias I-V characteristic of the n-CBIRD appears nearly diffusion limited, the p-CBIRD clearly is not. One possible explanation the observed difference is dopant migration. Nominally, the pN junction is at the absorber/hB SL interface. In the n-CBIRD, during growth, p dopants in the absorber can migrate into the hB SL grown on top of it, moving the junction into the wider gap hB SL. The opposite happens in the p-CBIRD, placing the junction in the narrow gap absorber region, which facilitates trap-assisted tunneling processes.

A prototype 1024×1024 focal plane array (FPA) without anti-reflection coating was fabricated using the p-CBIRD material. This initial array has a pixel operability of 96.3%. The measured FPA quantum efficiency is 21%. The cutoff wavelength is 11.5 μm. The noise equivalent differential temperature (NEΔT) of 53 mK was obtained at an operating temperature of 80 K, with 300 K background and cold-stop. An image taken with the first megapixel LWIR p-CBIRD SL camera is shown in Figure 5. The p-CBIRD FPA is reported in more detail in Reference 45. We have also fabricated a 320×256 format FPA based on the n-CBIRD design. Figure 6 shows a set of images taken with this FPA at an operating temperature of 78K. The 50%-responsivity cutoff wavelength for this array is 10 μm. Preliminary analysis indicates an operability of 98%, and an NEΔT of 26 mK with 300 K background.

4. CONCLUSIONS

The antimonide material system is relatively robust and has the potential for good manufacturability. The versatility of the material system, with the availability of three different types of band offsets, provides great flexibility in device design. In the MWIR, the use of unipolar barriers in the nBn design has already seen success. In the LWIR, type-II InAs/Ga(In)Sb superlattices have been shown theoretically to have reduced Auger recombination and suppressed band-

to-band tunneling. Suppressed tunneling allows for higher doping in the absorber, which has led to reduced diffusion dark current. Heterostructures such as those based on the CBIRD design have been used effectively to suppress G-R dark current. As a result, the dark current performance of antimonide superlattice based single element LWIR detectors are now approaching that of the state-of-the-art MCT detector, with sufficient performance for tactical applications and potential for strategic applications [46]. To date, the antimonide superlattices still have relatively short carrier lifetimes; this issue needs to be resolved before type-II superlattice infrared detectors can achieve their true potential. Reliable surface leakage current suppression methods, such as that based robust surface passivation, would be needed to achieve high-performance in focal plane arrays. Preliminary focal plane arrays results are highly encouraging.

Figure 6. Images taken with a 320×256 format LWIR n-CBIRD focal plane array at an operating temperature of 78K. The detector cutoff wavelength is 10 μm.

Acknowledgment

The authors thank C. J. Hill, S. Bandara, E. R. Blazejewski, D. R. Rhiger, and R. E. DeWames for helpful discussions, B. Yang and E. Luong for assistance, and M. Tidrow, R. Liang, M. Herman and E. Kolawa for encouragement and support. The research described in this publication was carried out at the Jet Propulsion Laboratory, California Institute of Technology, under a contract with the National Aeronautics and Space Administration.

REFERENCES

1. G. A. Sai-Halasz, R. Tsu, and L. Esaki, "A new semiconductor superlattice," *Appl. Phys. Lett.* **30**(12), 651-653 (1977).

2. G. A. Sai-Halasz, L. Esaki, and W. A. Harrison, " InAs-GaSb superlattice energy structure and its semiconductor-semimetal transition," *Phys. Rev. B* **18**(6), 2812–2818 (1978).

3. D. L. Smith and C. Mailhiot, "Proposal for strained type II superlattice infrared detectors," *Appl. Phys. Lett.* **34**(10), 663-665 (1987).

4. D. L. Smith, T. C. McGill, and J. N. Schulman "Advantages of the HgTe-CdTe superlattice as an infrared detector material," *Appl. Phys. Lett.* **43**(2), 180-182 (1983).

5. C. H. Grein, P. M. Young, and H. Ehrenreich, "Minority carrier lifetimes in ideal InGaSb/InAs superlattices," *Appl. Phys. Lett*. **61**(24), 2905 (1992).

6. E. R. Youngsdale, J. R. Meyer, C. A. Hoffman, F. J. Bartoli, C. H. Grein, P. M. Young, H. Ehrenreich, R. H. Miles, and D. H. Chow, "Auger lifetime enhancement in InAs-$Ga_{1-x}In_xSb$ superlattices," *Appl. Phys. Lett.* **64**(23), 3160-3162 (1994).

7. F. Fuchs, J. Wagner, J. Schmitz, N. Herres, and P. Koidl, "Growth and Characterization of InAs/AlSb/GaSb Heterostructures." in *Antimonide-related strained-layer heterostructures* (M. O. Manasreh, Ed.), pp. 191-232. Gordon Breach Science Publishers, Amsterdam (1997).

8. L. Bürkle and F. Fuchs, "InAs/(GaIn)Sb superlattices: a promising material system for infrared detection" in *Handbook of Infrared Detection Technologies* (M. Henini and M. Razeghi, Ed.), pp. 159-189. Elsevier Science, Oxford (2002).

9. L. Bürkle and F. Fuchs, "GaSb/InAs superlattices for infrared FPAs" in *Handbook of Infrared Detection Technologies* (M. Henini and M. Razeghi, Ed.), pp. 191-232. Elsevier Science, Oxford (2002).

10. David Z.-Y. Ting, Alexander Soibel, Linda Höglund, Jean Nguyen, Cory J. Hill, Arezou Khoshakhlagh, and Sarath D. Gunapala, "Type-II Superlattice Infrared Detectors" in *Semiconductors and Semimetals*, Vol. 82, *Advances in Infrared Photodetectors* (S. Gunapala, D. Rhiger, and C. Jagadish, Ed.), Elsevier (2011).

11. A. Rogalski, *Infrared Detectors*, CRC Press, Boca Raton (2011).

12. X. Cartoixà, D. Z.-Y. Ting, and T. C. McGill, "Description of bulk inversion asymmetry in the effective-bond-orbital model," *Phys. Rev. B* **68**(23), 235319 (2003).

13. C. H. Grein, P. M. Young, M. E. Flatte, and H. Ehrenreich, "Long wavelength InAs/InGaSb infrared detectors: Optimization of carrier lifetimes," *J. Appl. Phys*. **78**(12). 7143-7152 (1995).

14. C.H. Grein, and H Ehrenreich, "Improvement of infrared detector performance in carrier depleted strained layer type II superlattices," *J. Appl. Phys*. **82**(12), 6365-6367 (1997).

15. C.H. Grein, W. H. Laub , T. L. Harbertb, and M.E. Flatte, "Modeling of Very Long Infrared Wavelength InAs/GaInSb Strained Layer Superlattice Detectors," *Proc. SPIE* **4795**, 39-43. (2002).

16. M.E. Flatte and C.H. Grein, "Theory and modeling of type-II strained-layer superlattice detectors," *Proc. SPIE* **7222**, 72220Q (2009).

17. D. Z.-Y. Ting, S. V. Bandara, J. Mumolo, S. A. Keo, J. Nguyen, H.C. Liu, C.Y. Song, Y.-C. Chang, S. B. Rafol, C. J. Hill, S. D. Gunapala, A. Soibel, J. K. Liu, E. Blazejewski, "Dots, QWISPs, and BIRDs," *Infrared Physics & Technology*, **52**(6), 294-298 (2009).

18. David Z.-Y. Ting, Sumith V. Bandara, Cory J. Hill, Sarath D. Gunapala, Yia-Chung Chang, H. C. Liu, C. Y. Song, Alexander Soibel, Jason Mumolo, Jean Nguyen, John K. Liu, Sam A. Keo, Sir B. Rafol, and E. R.

Blazejewski, "Novel quantum well, quantum dot, and superlattice heterostructure based infrared detectors", *Infrared Technology and Applications XXXV*, edited by Bjørn F. Andresen, Gabor F. Fulop, Paul R. Norton, *Proc. of SPIE* Vol. **7298**, 729805, (2009).

19. D. Z.-Y. Ting, C. J. Hill, A. Soibel, S. A. Keo, J. M. Mumolo, J. Nguyen, and S. D. Gunapala, "A high-performance long wavelength superlattice complementary barrier infrared detector," *Appl. Phys. Lett*. **95**, 023508 (2009).
20. H. Kroemer, "A proposed class of heterojunction injection lasers," *Proc. IEEE* **51**(12), 1782 (1963).
21. Zh. I. Alferov, R. F. Kazarinov, Inventor's Certificate No. 181737 (in Russian), Application No. 950 840 (1963).
22. S. Maimon and G. W. Wicks, "InAsSb/GaAlSb/InAsSb nBn IR detector for the 3-5μm", 11th International Conference on Narrow Gap Semiconductors, June 16-20, 2003, Buffalo, New York (abstract only).
23. S. Maimon and G. W. Wicks, "nBn detector, an infrared detector with reduced dark current and higher operating temperature," *Appl. Phys. Lett*. **89**(15) 151109 (2006).
24. J. R. Pedrazzani, S. Maimon and G. W. Wicks, "Use of nBn structures to suppress surface leakage currents in unpassivated InAs infrared photodetectors," *Electronics Lett*. **44**(25) 1487-1488 (2008).
25. P.C. Klipstein, "Depletion-less Photodiode with Suppressed Dark Current and Method for Producing the Same" Int. Patent Publication no: WO 2005/004243 A1 (13 January 2005, priority date: 2 July 2003)
26. P. Klipstein, "'XBn' barrier photodetectors for high sensitivity and high operating temperature infrared sensors," *Proc. of SPIE*. 6940 (2008) 69402U.
27. Olga Klin, Steve Grossman, Noam Snapi, Maya Brumer, Inna Lukomsky, Michael Yassen, Boris Yofis, Alex Glozman, Ami Zemel, Tal Fishman, Eyal Berkowitz, Osnat Magen, Joelle Oiknine-Schlesinger, Itay Shtrichman, Eliezer Weiss and P C Klipstein, "Progress with Antimonide Based Detectors at SCD" Proc. Infrared Technology and Applications XXXV, SPIE 7298, 7298-0G (2009).
28. Philip Klipstein, Olga Klin, Steve Grossman, Noam Snapi, Barak Yaakobovitz, Maya Brumer, Inna Lukomsky, Daniel Aronov, Michael Yassen, Boris Yofis, Alex Glozman, Tal Fishman, Eyal Berkowicz, Osnat Magen, Itay Shtrichman, and Eliezer Weiss, " 'XBn' Barrier Detectors for High Operating Temperatures", Proc. of SPIE Vol. 7608, 76081V (2010).
29. J. B. Rodriguez, E. Plis, G. Bishop, Y. D. Sharma, H. Kim, L. R. Dawson, and S. Krishna, "nBn detectors based on InAs/GaSb type-II strain layer superlattice," *Appl. Phys. Lett*. **91**(4) 043514 (2007).
30. A. Khoshakhlagh, J. B. Rodriguez, E. Plis, G. D. Bishop, Y. D. Sharma, H. S. Kim, L. R. Dawson, and S. Krishna, "Bias dependent dual band response from InAs/Ga(In)Sb type II strain layer superlattice detectors," *Appl. Phys. Lett.* **91**, 263504 (2007).
31. B.-M. Nguyen, S. Bogdanov, S. Abdollahi Pour, and M. Razeghi, "Minority electron unipolar photodetectors based on type II InAs/GaSb/AlSb superlattices for very long wavelength infrared detection", *Appl. Phys. Lett*. **95**, 183502 (2009).
32. A. D. Hood, A. J. Evans, A. Ikhlassi, D. L. Lee, and W. E. Tennant, "LWIR Strained-Layer Superlattice Materials and Devices at Teledyne Imaging Sensors," *J. Electron. Mater.* **39** (7), 1001-1006. (2010).
33. I. Vurgaftman, E. H. Aifer, C. L. Canedy, J. G. Tischler, J. R. Meyer, J. H. Warner, E. M. Jackson, G. Hildebrandt and G. J. Sullivan, "Graded band gap for dark-current suppression in long-wave infrared W-structured type-II superlattice photodiodes," *Appl. Phys. Lett*. **89**(12), 121114 (2006).
34. Delaunay, P.-Y., Hood, A., Nguyen, B. M., Hoffman, D., Wei, Y., and Razeghi, M. (2007a). Passivation of type-II InAs/GaSb double heterostructure, *Appl. Phys. Lett.* **91**, 091112.

35. Nguyen, B.-M., Hoffman, D., Delaunay, P.-Y., and Razeghi, M. (2007b). Dark current suppression in type II InAs/GaSb superlattice long wavelength infrared photodiodes with M-structure barrier. *Appl. Phys. Lett.* **91**(16) 163511.

36. Gautam, N., Kim, H.S., Kutty, M. N., Plis, E., Dawson, L.R., and Krishna, S. (2010). Performance improvement of longwave infrared photodetector based on type-II InAs/GaSb superlattices using unipolar current blocking layers, *Appl. Phys. Lett.* **96**, 231107.

37. Dmitry Donetsky, Stefan P. Svensson, Leonid E. Vorobjev, and Gregory Belenky, "Carrier lifetime measurements in short-period InAs/GaSb strained-layer superlattice structures", Appl. Phys. Lett. 95, 212104 (2009)

38. Connelly, B. C., Metcalfe, G. D., Shen, H., and Wraback, M. (2010). Direct minority carrier lifetime measurements and recombination mechanisms in long-wave infrared type II superlattices using time-resolved photoluminescence. *Appl. Phys. Lett.* **97**(25), 251117.

39. Pellegrino, J., DeWames, R. (2009). Minority carrier lifetime characteristics in type II InAs/GaSb LWIR superlattice n+π p+ photodiodes. *Proc. SPIE* **7298**, 72981U-4.

40. Edwall, D. D., DeWames, R. E., McLevige, W. V., Pasko, J. G., and Arias, J. M. (1998). Measurement of minority carrier lifetime in n-type MBE HgCdTe and its dependence on annealing. *J. Electron. Mater.* **27**(6), 698.

41. Kinch, M. A., Aqariden, F., Chandra, D., Liao, P-K, Schaake, H. F. and Shih, H. D. (2005). Minority carrier lifetime in p-HgCdTe. *J. Electron Mater.* **34**(6), 880.

42. Linda Höglund, Alexander Soibel, Cory J. Hill, David Z. Ting, Arezou Khoshakhlagh, Anna Liao, Sam Keo, Michael C. Lee, Jean Nguyen, Jason M. Mumolo, Sarath D. Gunapala, "Optical studies on antimonide superlattice infrared detector material", *Proc. SPIE* **7780**, 77800D (2010).

43. Alexander Soibel, David Z.-Y. Ting, Cory J. Hill, Mike Lee, Jean Nguyen, Sam A. Keo, Jason M. Mumolo, and Sarath D. Gunapala, "Gain and noise of high-performance long wavelength superlattice infrared detectors", *Appl. Phy. Lett.* **96**(11), 111102 (2010).

44. Jean Nguyen, Alexander Soibel, David Z.-Y. Ting, Cory J. Hill, Mike C. Lee, and Sarath D. Gunapala, "Low dark current long-wave infrared InAs/GaSb superlattice detectors", *Appl. Phy. Lett.***97**(5), 051108 (2010).

45. S. D. Gunapala, D. Z. Ting, C. J. Hill, J. Nguyen, A. Soibel, S. B. Rafol, S. A. Keo, J. M. Mumolo, M. C. Lee, J. K. Liu, and B. Yang, "Demonstration of a 1024x1024 Pixel InAs–GaSb Superlattice Focal Plane Array", *IEEE Photonics Technol. Lett.* **22**(24) 1856-1858 (2010).

46. Sumith V. Bandara, "Performance Analysis of InAs/Ga(In)Sb Strained Layer Superlattice Detectors and Focal Plane Arrays", *Proc. of SPIE* **7608**, 76081M (2010).